

# UNVEILING THE STRUCTURAL RESPONSE OF THE RIBCAGE: CONTRIBUTION OF THE INTERCOSTAL MUSCLES TO THE THORACIC MECHANICAL RESPONSE

**David Poulard**

Center for Applied Biomechanics, University of Virginia  
USA

**Damien Subit**

Institut de Biomécanique Humaine Georges Charpak, Arts et Métiers ParisTech  
France

Paper Number 15-0387

## ABSTRACT

Current finite element (FE) models of the human body do not properly include the contribution of the intercostal muscles (ICM), which is believed to limit their rib fracture prediction capabilities. In the present study, an existing full body model for a seated 50th-percentile male was evaluated under five cases of loading: point loading of the denuded ribcage, frontal pendulum impact tests, lateral and oblique pendulum impact tests and table top tests. The sensitivity of the model to changes in material model of the ICM was evaluated by using two material models: an isotropic linear elastic material model and a foam model defined by a single uniaxial load curve extracted from a recent literature. The performance of these models compared to the experiments was assessed quantitatively through a correlation analysis on the force and chest deflection time histories. The simulations found that the material properties of the ICM have little effect on the externally measured impact force and chest deformation except in point loading.

## INTRODUCTION

Thoracic injuries are the most common blunt trauma sustained by restrained occupants in motor vehicle crashes [1]. Amongst thoracic injuries, rib fractures are commonly used as an indicator of a crash severity as these fractures are relatively straight forward to detect and the increase of their number was shown to be associated to an increase of the risk of sustaining more severe injuries to the internal organs (aorta, lungs, heart). The structure of the thoracic segment structure is complex because of its geometry and the material heterogeneity: it consists of the ribcage, the viscera, the musculature and the skin, and its mechanical response results from the contribution of these tissues, soft and hard. Understanding how the thorax deforms under dynamic solicitations is an active area of research.

Finite element (FE) models of the human thorax or the entire body have been developed to investigate the structural response of the thorax and establish its injury tolerance [2-9]. These models rely on two types of data: the material and geometrical information to build them, and the experimental data required to evaluate their biofidelity, i.e. their ability to predict a mechanical response under dynamic loading similar to what would experience a real person. In both cases, post-mortem human (PMHS) data are used, and the capabilities of the models depend on the availability of the experimental data.

Material constitutive models and the required data to validate the models created for the isolated thoracic components are available for nearly all the tissues: clavicle [10, 11], ribs [12-14] and costal cartilage [15, 16]. However, there is little information in the literature for the intercostal muscles (ICM), and therefore the FE models currently available use material properties reported on in by [17]. This study lists properties of some thoracic muscles, such as the pectoralis major and the trapezius but not specifically identify intercostal material properties. Therefore, as thoracic muscle structure differs along the thorax, modeling the ICM using properties of other thoracic muscles may be not appropriate. It was found from animal experiments that the intercostal muscles could generate substantially less tensile force than other muscles like the diaphragm [18, 19]. Recently, Kindig et al. [20] found that decreasing the elastic modulus of the intercostal muscles of a FE ribcage model alter significantly the ribcage

deformation under quasi-static point loading and dynamic sternal loading. Moreover, while an isotropic linear elastic material model is commonly used for modeling the ICM, it was found from cadaver tests that ICM exhibit a hyperelastic behavior in tension [21]. Thus, it appears that the FE models currently available do not properly include the contribution of the intercostal muscles, which is believed to limit the rib fracture prediction capabilities of the thorax model.

Therefore, the goal of this present study is to examine the sensitivity of a thorax FE to the changes in intercostal muscle material constitutive model based on recent literature. To do, a parametric analysis was performed to evaluate the sensitivity of the thorax to the constitutive models used for the ICM using a human body model (HBM). The different versions of the HBM were exercised under several loading conditions with various constitutive models for the ICM and their performance was assessed quantitatively to experiments through a correlation analysis.

## **METHODOLOGY**

### **Finite Element Body Model Overview**

The HBM used in this study was the version 4.1 of the seated 50th-percentile male, developed in LS-DYNA for the Global Human Body Models Consortium (GHBMC). This full model has been described in a previous study [9, 14, 22] and evaluated under various loading environments (antero-posterior rib bending, point loading of the denuded ribcage, omnidirectional pendulum impact and table top) through a correlation metric tool (CORA) based on linearly independent signals [9].

The intercostal muscles were defined as a single layer of triangular planar shell elements of 1.5 mm thickness which were attached between adjacent ribs. The membrane element formulation was used since it was assumed that the intercostal could not support a through-thickness bending load. By default, an isotropic linear elastic material model with  $E=0.5$  MPa, was used for these elements. This material model was changed in the present study.

### **Defining new material properties for the intercostal muscles**

Material Type 181 (\*MAT\_SIMPLIFIED\_RUBBER/FOAM) was used for a new model of the behavior of the ICM. This material model provides a rubber and foam model defined by a single uniaxial load curve defining the force versus actual change in a gauge length. The single uniaxial load curve was defined to cover the complete range of expected loading.

In tension, the load curve was defined from the hyperelastic behavior of the ICM found in [21]. In this study, tensile tests were performed on three ICM samples harvested from one cadaver at different locations: one sample (#A) located between ribs 8 and 9 from the anterior aspect of the rib cage, and two samples (#B and #C) located between ribs 9 and 10 in the lateral and posterior aspects of the rib cage. For the three samples, a toe region was observed, followed by quasi-linear response after about 30 % of stretch and failure at 60%. An average stress-strain response from the three samples was extracted and converted to a load-displacement curve by assuming a specimen gauge length, width and thickness of 1 mm.

Figure 1 shows the stress-strain curve used in the rubber/foam model, the experimental curves used for its definition and the stress-strain curve based on the default material for comparison. In compression, the load curve was defined to eliminate the compressive action since the ICM exhibit similar behavior [21]. Nevertheless, stiffen up the material stress-strain curve at large compression ( $\epsilon < 0.8$ ) was found essential for avoiding negative volume.

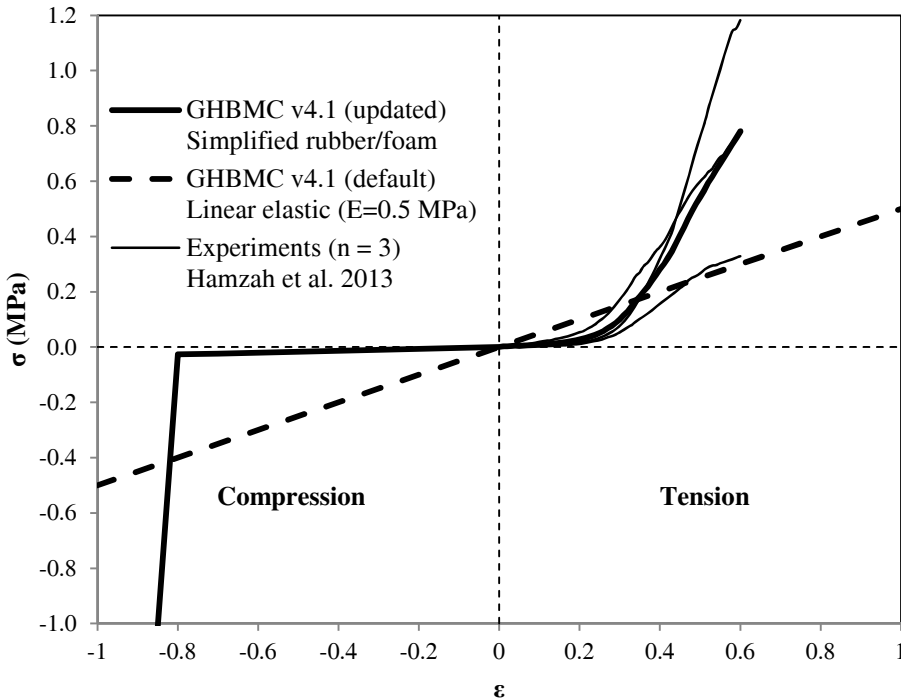


**Figure 1.** Stress-strain curves used in the ICM for the updated version the GHBMC model, the experimental curves used for its definition and the stress-strain curve based on the default material for comparison.

### Evaluation cases

The influence of the ICM material on thoracic mechanical response was evaluated from the denuded ribcage to the full body model using four sets of experiments. These experimental cases were selected based on their previous use for the validation of the HBM [9]. The experimental tests and model validation process are described below.

**Point loading of the eviscerated ribcage** Quasi-static point loading of the ribcage was simulated, using the method outlined in Kindig et al. [23]. The FE model of the ribcage was positioned oriented in an upright position similar to the experiment and the six degrees of freedom of the thoracic vertebrae were constrained. The spherical segment was positioned and oriented such that the contact surfaces on the sphere did not initially penetrate the ribcage mesh (Figure 2a). The loading plate was positioned initially in contact with the contact surface of the sphere and aligned such that the vector normal to the plate was directed along the average vector direction used in the experiments at this particular loading location. The plate was constrained to translate along this vector only, with no rotation allowed, consistent with the experimental boundary conditions. The plate was displaced at a constant 200 mm/sec up to the prescribed displacement used in the experiment (varied with the loading location). The loading rate to 200 mm/sec provided a reasonable simulation time while maintaining stable contact forces. To avoid strain-rate effects, the Cowper-Symonds yield-stress scaling in the bone material models was disabled. The reaction force onto the plate nodes was outputted for comparison with experiment.

Simulations were performed at the lower and upper sternum levels and the costochondral junction (CCJ) of rib levels 1, 3, 4, 6, and 9 (Figure 2b). The average value of the maximum normalized displacement obtained in experiments for each location was used to define the maximum displacement reached in simulation and

consequently the termination time. No modifications were made on the force and displacement obtained from simulations.

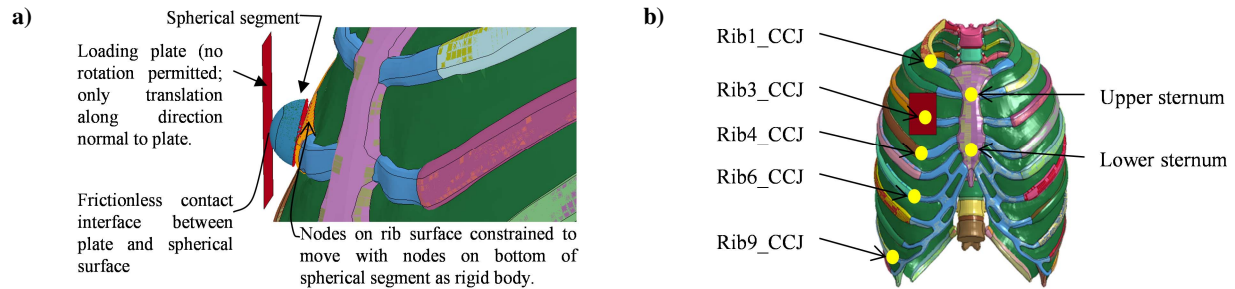


**Figure2.** Setup for point loading simulation [9]. (a) Close-up at loading site (b) anterior view.

**Frontal pendulum impact** The FBM was exercised under frontal pendulum impact [24]. In the simulation, the FBM was seated on a rigid plate and the impactor positioned at the midsternum level (Figure 3a). An initial velocity of 4.3 m/s was imposed on the impactor. The impact force was measured as the contact force between the impact and model. Chest deflection was defined as the variation of length between the middle of two nodes taken on the pectoral muscles and a node taken on the skin at T8 level [9]. The impact force chest deflection curve from the FE model simulations was compared to the experimental corridors normalized to the 50th percentile male developed by Lebarbé and Petit [25] to evaluate the response of the thorax model.

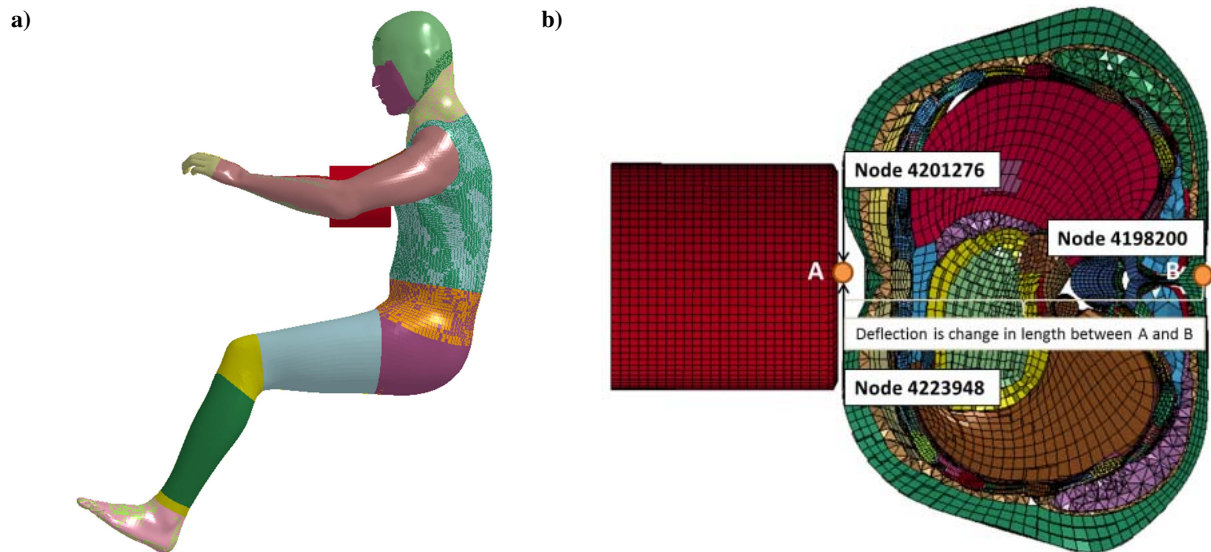


**Figure3.** Setup for frontal pendulum impact [9]. (a) Lateral view, (b) Superior view of the cross-section of the thorax at the mid-sternum showing the points used to measure the chest deflection.

**Pure lateral impact** The FBM was further run according to a pure lateral impact configuration available in the literature [26]. In the simulation, the FBM was seated on a rigid plate and the impactor positioned under the axillary level, similar to the experiments (Figure 4a). The cylindrical impactor with a diameter of 152 mm, a mass of 23.4 kg and an initial impact velocity of 2.5 m/s was centered with the transverse plane through the fourth interspace of the ribcage. The impact force was measured as the contact force between the impactor and model. The chest deflection was defined as the change in length between two bilateral nodes aligned with the center of the impactor (Figure 4b).

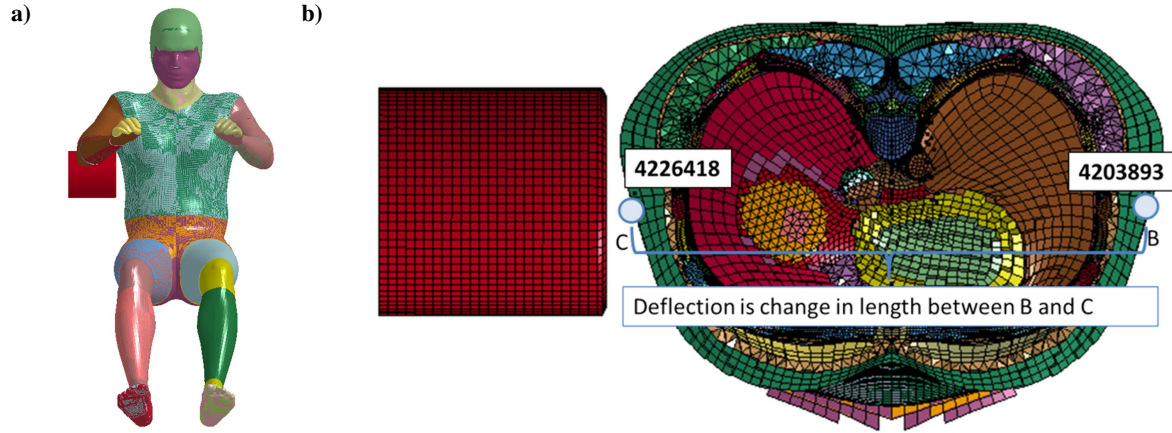


**Figure 4.** Setup for lateral pendulum impact [9]. (a) Frontal view, (b) Superior view of the cross-section of the thorax at the level of sternum the fourth interspace showing the points used to measure the chest deflection.

In a qualitative evaluation, the force-deflection curve from the FE model was compared to the experimental corridors normalized to the 50th percentile male developed by Shaw et al. [26]. For the quantitative evaluation, the force/time and deflection/time histories were used.

**Table top tests** The FBM was set-up to simulate four tabletop restrained configurations [27]:

- hub loading, where the hub was simulated as a cylindrical rigid body with a diameter of 152 mm,
- belt loading, where single and double diagonal belts were modeled by a layer of 2-mm thick shell elements,
- distributed loading, where an extra-wide belt was modeled by a layer of 2-mm-thick shell elements and was 203-mm wide.

The pulley system used in the experiments was simulated by slip ring elements and several 1-D belt elements so that the loading angles of the 1D-belt elements were maintained and consistent with experimental configurations (Figure 6a). These tabletop models were loaded using the displacement-time history reported on in Kent et al. [27] up to 20% of chest compression (non-injurious level) for all the four loading conditions (Figure 6b). The displacement was applied symmetrically to the extremities of the single, double and distributed loading, and to the hub. Prior to applying the loading, the models were allowed to settle on the table for 100 ms under its own weight. The settling process was applied in a pre-simulation and the initial stress was imported in the FBM for the table top simulations. The limbs were cut to reduce the computation time.

The reaction force was defined as the contact force between the support table and the model. The compression was defined as the ratio of the Z-displacement of a node taken on midsternum (A, Figure 6a) divided by the initial distance between A and the support table.

The reaction force versus compression curves were then compared to the thoracic response corridors developed from the fifteen PMHS tested by Kent et al. [27].

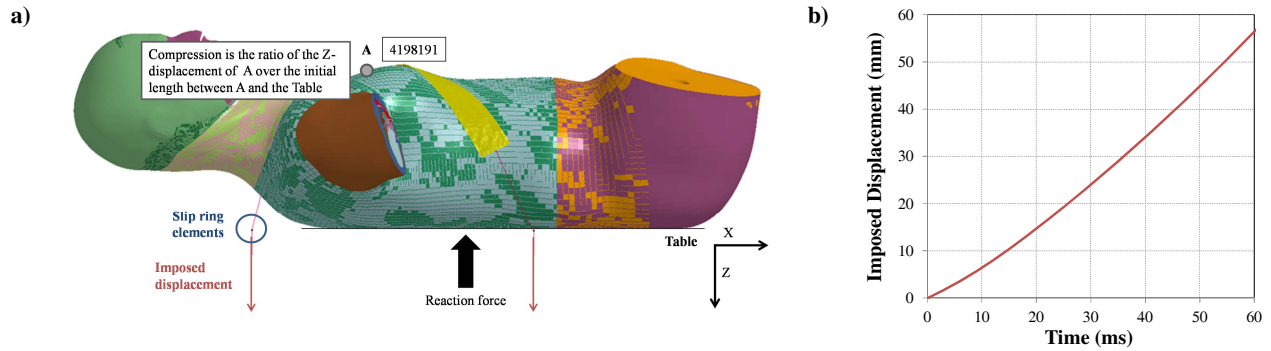


**Figure5. Setup for single belt table top test [9]. (a) Lateral view, (b) Displacement imposed to the loading structure.**

### Quantitative assessment of the response of the model

A quantitative assessment of the response of the models compared to the five sets of experiments was performed through metrics obtained with the CORA software (CORelation and Analysis, Partnership for Dummy Technology and Biomechanics). Each of these metrics is given a score and the weighed sum of these score is the CORA score ranging between 0 and 1. A CORA score above 0.8 is considered as a good fit between the model and the experimental response [28]. As CORA calculates the correlation of each signal separately, those single ratings were combined to a global model rating by calculating the mean value of all the ratings. Table 1 shows which data were used to establish the rating for each load cased. Ratings with a score of 0.8 or higher were assumed as good.

The experimental response was defined from the average response and inner/outer corridors derived from the experimental results [9].

**Table1.**  
**Signals used in the correlation analysis [9].**

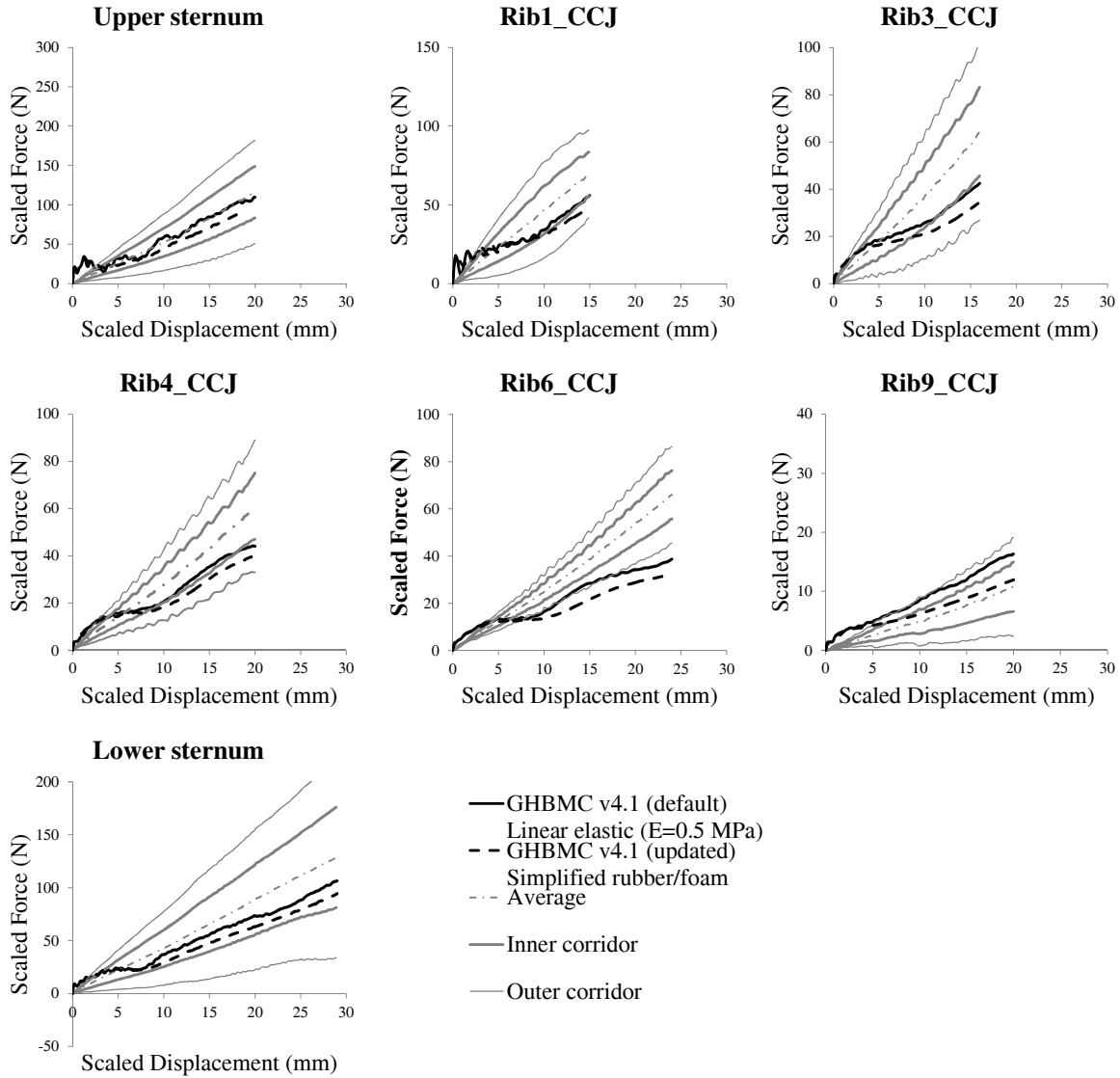
Load case	Sub load case(s)	Signals
Point loading of the ribcage	Lower sternum, Rib1_CCJ, Rib3_CCJ, Rib4_CCJ, Rib6_CCJ, Rib9_CCJ, Upper sternum	1. Force vs. Displacement*
Frontal pendulum impact	Impact velocity 4.3 m/s	1. Force vs. Time 2. Deflection vs. Time
Lateral pendulum impact	Impact velocity 2.5 m/s	1. Force vs. Time 2. Deflection vs. Time
Table top	Hub, Single Belt, Double Belt, Distributed Loading	1. Force vs. Compression*

\*: Equivalent to Force vs. Time in CORA, as displacement and chest compression were the independent variables.

## RESULTS

### Point loading of the eviscerated ribcage

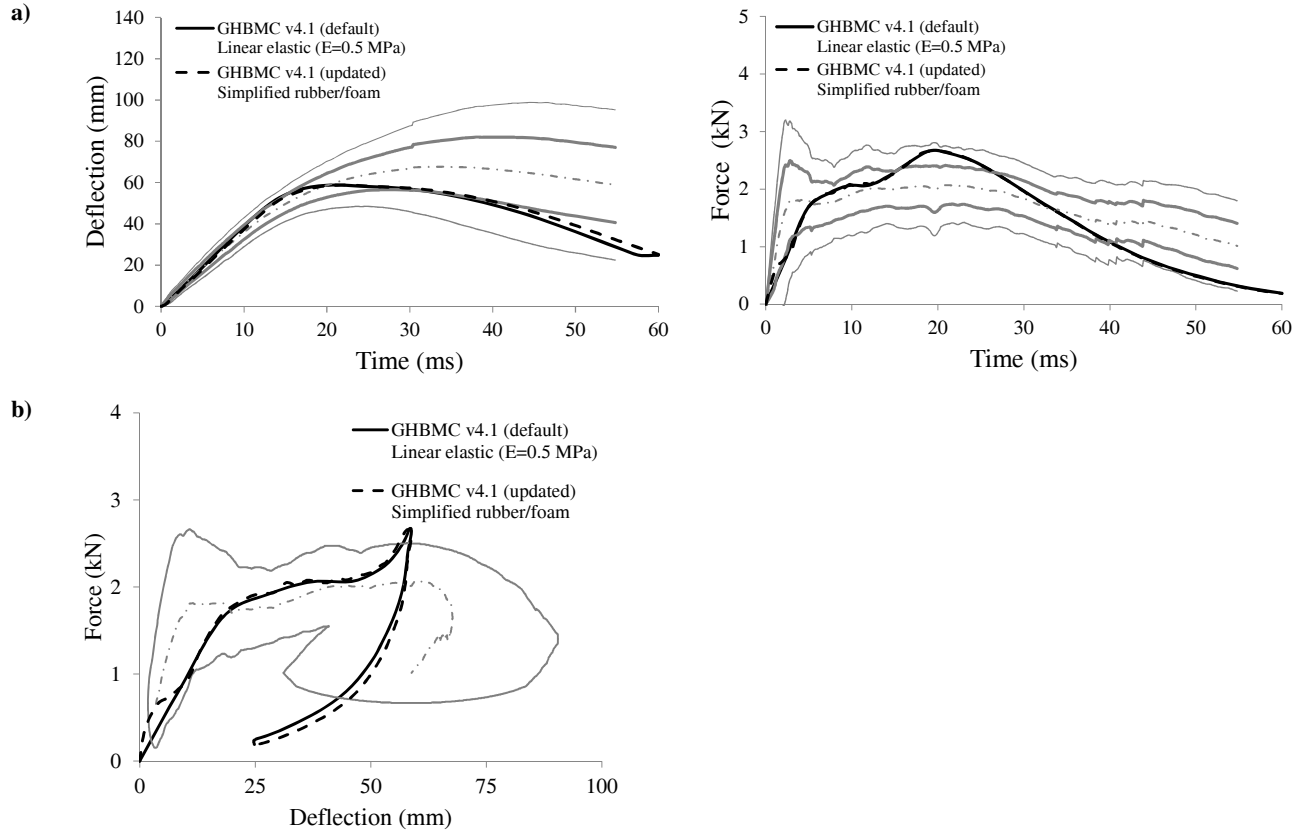
The scaled force versus scaled deflection curves predicted by the HBM after ICM modification different from the baseline model (Figure 6). In all tested locations, the model after modification was found to be more compliant, up to be out of the corridors. Quantitatively, the average CORA model score was  $0.73 \pm 0.12$  after modification was lower than the baseline model ( $0.80 \pm 0.12$ )(Table 2).



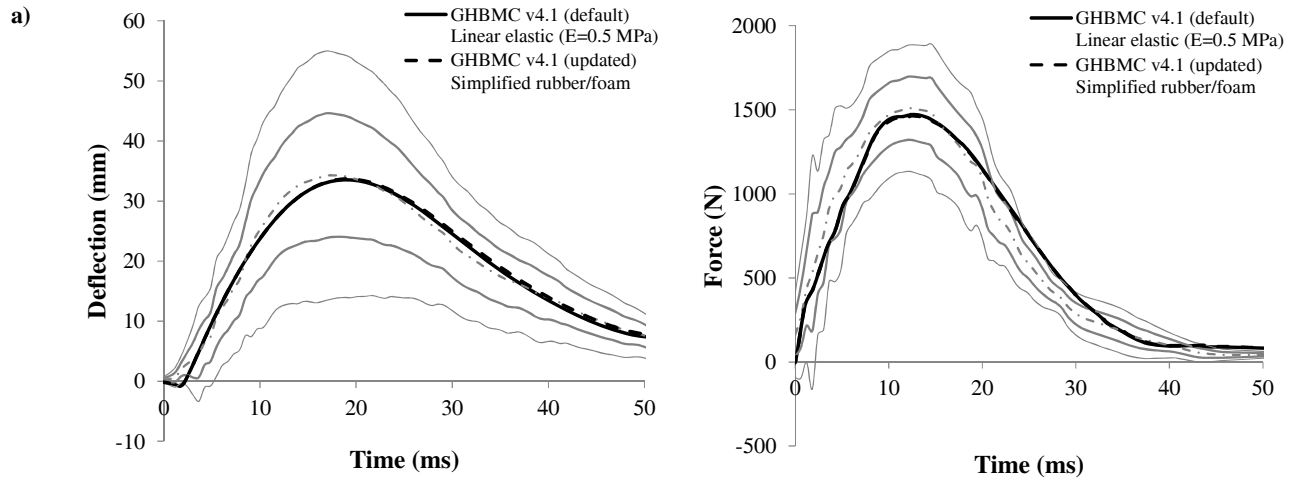
**Figure6. Model performance for point loading of the denuded ribcage. Scaled Force-Scaled Displacement. Experimental corridors are adapted from [23].**

**Frontal and lateral pendulum tests**

The reaction force versus chest deflection curves predicted by the HBM after ICM modifications was really close to the baseline model (Figure 7 and 8). CORA model scores after modifications were 0.86 in frontal and 0.89 in lateral close to the scores obtained with the baseline model (0.84 and 0.89 respectively) (Table 2).



**Figure 7. Model performance for frontal pendulum tests. (a) Deflection-Time and Force-Time histories, (b) Force-Deflection, (c) CORA ratings. Experimental corridors are adapted from [24] and [25].**



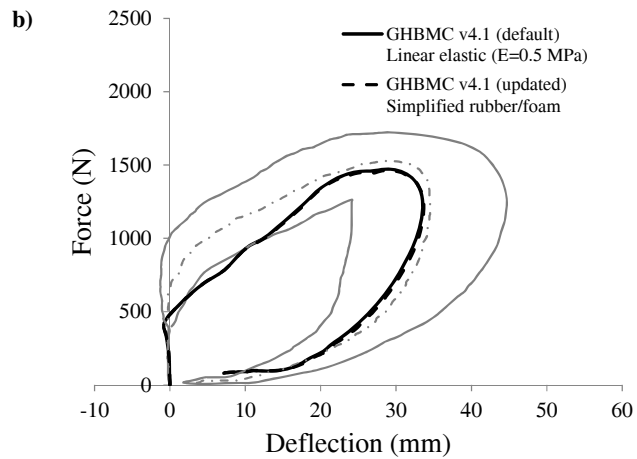


**Figure8.** Model performance for lateral pendulum tests: (a) Deflection-Time and Force-Time histories, (b) Force-Deflection. Experimental corridors are adapted from [26].

#### Table top tests

The reaction force versus chest compression curves predicted by the HBM after modifications closely agreed with the response obtained by the baseline model for all configurations (Figure9). The average CORA model score obtained by the model after modifications was  $0.83 \pm 0.10$ , slightly lower than the baseline model ( $0.86 \pm 0.10$ ) (Table 2).

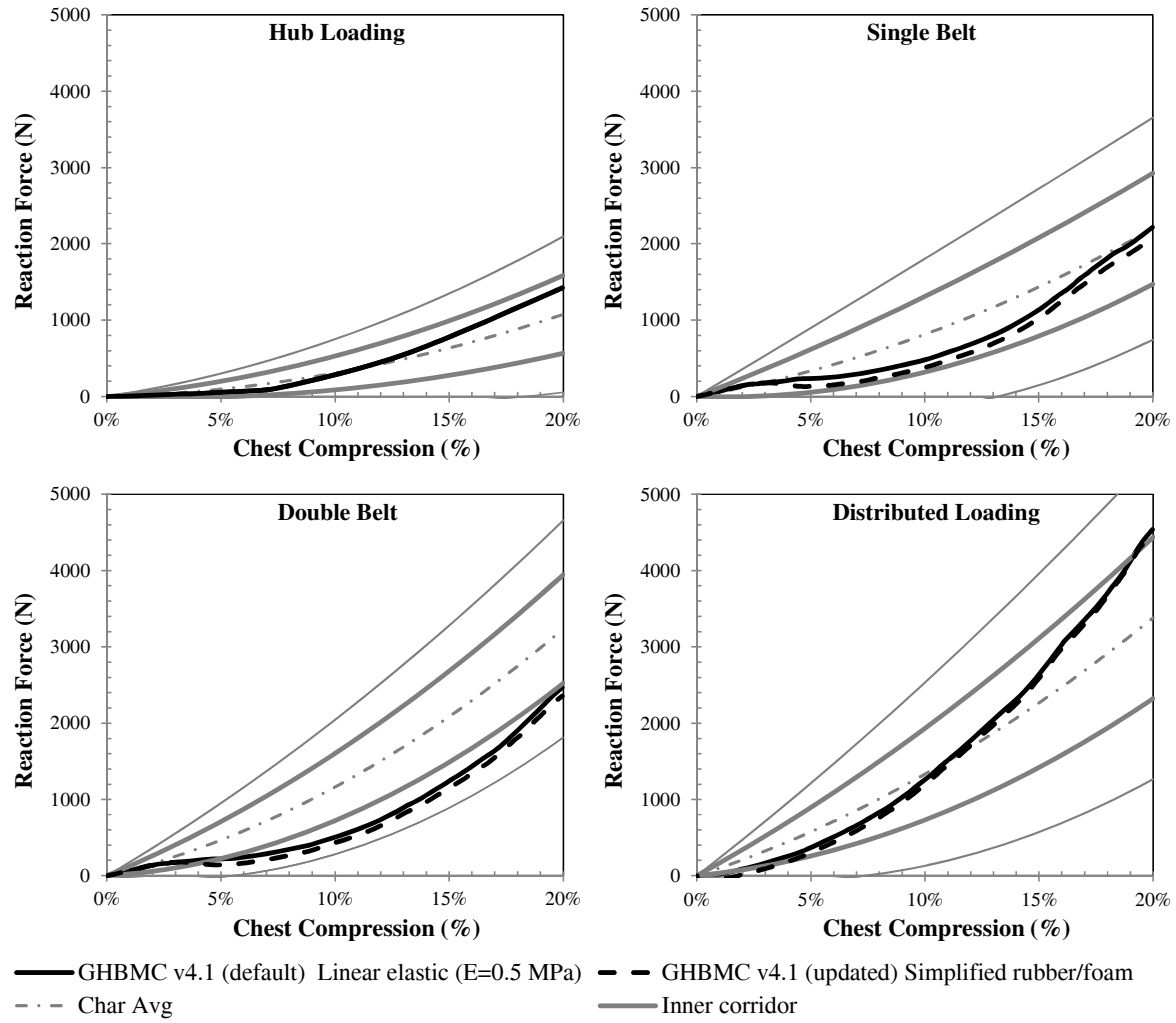


**Figure 9. Model performance for table top tests. (a) Reaction Force-Chest Compression, (b) CORA ratings. Experimental corridors are adapted from [27].**

**Table2.**  
**CORA scores.**

Model	Subload Case	Signal	Corridor Score	Cross-correlation				Signal Score	Model Score
				Phase Score	Size Score	Progression Score	Score		
Point loading of the ribcage	1*	Lower sternum	Force	1.00	<i>Ignored</i>	0.54	1.00	0.77	0.89
		Rib1_CCJ	Force	0.89	<i>Ignored</i>	0.51	0.98	0.75	0.82
		Rib3_CCJ	Force	1.00	<i>Ignored</i>	0.31	0.99	0.65	0.83
		Rib4_CCJ	Force	0.93	<i>Ignored</i>	0.46	0.99	0.73	0.83
		Rib6_CCJ	Force	0.44	<i>Ignored</i>	0.41	1.00	0.70	0.57
		Rib9_CCJ	Force	0.44	<i>Ignored</i>	0.93	1.00	0.96	0.70
		Upper sternum	Force	1.00	<i>Ignored</i>	0.79	1.00	0.90	0.95
	2**	Lower sternum	Force	1.00	<i>Ignored</i>	0.44	1.00	0.72	0.86
		Rib1_CCJ	Force	0.86	<i>Ignored</i>	0.50	0.97	0.74	0.80
		Rib3_CCJ	Force	0.85	<i>Ignored</i>	0.22	0.98	0.60	0.72
		Rib4_CCJ	Force	0.72	<i>Ignored</i>	0.35	0.99	0.67	0.69
		Rib6_CCJ	Force	0.15	<i>Ignored</i>	0.27	0.99	0.63	0.39
		Rib9_CCJ	Force	0.69	<i>Ignored</i>	0.77	0.98	0.87	0.78
		Upper sternum	Force	0.99	<i>Ignored</i>	0.56	1.00	0.78	0.88
Frontal	1	N/A	Deflection	0.89	<i>Ignored</i>	0.68	0.99	0.84	0.86
			Force	0.67	<i>Ignored</i>	0.94	0.98	0.96	0.82
	2	N/A	Deflection	0.93	<i>Ignored</i>	0.70	0.99	0.85	0.89
			Force	0.67	<i>Ignored</i>	0.95	0.98	0.96	0.82
Lateral	1	N/A	Deflection	0.97	<i>Ignored</i>	0.99	1.00	1.00	0.98
			Force	0.61	<i>Ignored</i>	1.00	1.00	1.00	0.80
	2	N/A	Deflection	0.96	<i>Ignored</i>	0.98	1.00	0.99	0.98
			Force	0.61	<i>Ignored</i>	1.00	1.00	1.00	0.80
Table top	1	Hub loading	Force	1.00	<i>Ignored</i>	0.64	1.00	0.82	0.91
		Single belt	Force	1.00	<i>Ignored</i>	0.74	0.91	0.83	0.91
		Double belt	Force	0.73	<i>Ignored</i>	0.40	0.99	0.70	0.71
		Distributed loading	Force	0.98	<i>Ignored</i>	0.71	1.00	0.85	0.92
	2	Hub loading	Force	1.00	<i>Ignored</i>	0.65	0.99	0.82	0.91
		Single belt	Force	1.00	<i>Ignored</i>	0.62	0.99	0.80	0.90
		Double belt	Force	0.58	<i>Ignored</i>	0.36	0.99	0.67	0.63
		Distributed loading	Force	0.89	<i>Ignored</i>	0.73	0.99	0.86	0.88

\* 1: GHBM v4.1 (default) | Linear elastic (E=0.5 MPa). \*\* 2: GHBM v4.1 (updated) | Simplified rubber/foam.

## **DISCUSSION**

The version 4.1 of the GHBM model was modified to include more realistic material definition of the intercostal muscles (ICM) based on recent published experiments. Its performance was evaluated qualitatively and quantitatively by comparison of the simulation results to the experiments based on signal correlation analysis. Overall, the material properties of the ICM have little effect on the externally measured impact force and chest deformation except in point loading. Sensitivity of the ICM in point loading was already observed in a previous study [20], but it is the first time such influence is studied on a thorax model at multiple length scales.

The use of a correlation method such as CORA allows to perform a multi-configuration evaluation of a FE model, and it is the first time such a method is applied to evaluate the influence of modification on a thorax model at multiple length scales. Nevertheless, not all the CORA ratings obtained for each test configuration was high, therefore a degree of caution is needed when we evaluated the influence of a specific parameter. Consequently, the relative assessment of different versions of the same model using CORA may be more pertinent than an absolute evaluation of a specific version. Thus, this method was used during this study for the different versions of the model.

As the current assessment of the model response focused on global response, its ability to predict rib fracture, a common feature in whole body FE models, was not evaluated. Fractures were reported in some tests but not in the point loading of the eviscerated ribcage which is the only load case displaying a sensitivity to a change in ICM material. An interesting contribution of this study will be to report the strain distribution within the ribcage to evaluate the influence of the ICM. Nevertheless, as no experimental data is currently available to evaluate strain distribution biofidelity, it will not be possible to assess the capability of the model to appropriately predict the strain distribution in the ribs for these loading cases.

## **CONCLUSIONS**

In the present study, an existing full body model for a seated 50th-percentile male was evaluated under five cases of loading: point loading of the denuded ribcage, frontal pendulum impact tests, lateral and oblique pendulum impact tests and table top tests. The sensitivity of the model to changes in material model of the intercostal muscles (ICM) was evaluated by using two material models: an isotropic linear elastic material model and a foam model defined by a single uniaxial load curve extracted from a recent literature. The performance of these models compared to the experiments was assessed quantitatively through a correlation analysis on the force and chest deflection time histories. The simulations found that the material properties of the ICM have little effect on the externally measured impact force and chest deformation except in point loading suggesting that the ICM has a localized effect. This localized effect may be captured by analyzing the strain distribution in the ribcage.

## **ACKNOWLEDGEMENTS**

The funding for this study was provided by the Global Human Body Models Consortium.

## **REFERENCES**

- [1] Carroll, J., et al. 2009. "A comparison between crash test results and real-world accident outcomes in terms of injury mechanisms and occupant characteristics." THORAX project GA (218516).
- [2] Robin, S. 2001. "HUMOS: human model for safety—a joint effort towards the development of refined human-like car occupant models." In Proceedings of the 17th Enhanced Safety of Vehicles Conference.
- [3] Iwamoto, M., et al. 2002. "Development of a finite element model of the total human model for safety (THUMS) and application to injury reconstruction." In Proceedings of the International Research Council on the Biomechanics of Injury conference.
- [4] Kimpara, H., et al., 2005. "Development of a Three-Dimensional Finite Element Chest Model for the 5 (th) Percentile Female"

- Stapp Car Crash J. 49: p. 251-269.
- [5] Zhao, J. and G. Narwani. 2005. "Development of a human body finite element model for restraint system R&D applications."  
In the 19th International Technical Conference on the Enhanced Safety of Vehicles (ESV).
- [6] Song, E., Trosseille, X. and Baudrit P. 2009. "Evaluation of thoracic deflection as an injury criterion for side impact using a finite elements thorax model."  
Stapp Car Crash J, 53: p. 155-191.
- [7] Ito, O., Dokko Y., and Ohashi K. 2009. "Development of adult and elderly FE thorax skeletal models."  
SAE Technical Paper.
- [8] Vezin, P. and Berthet F. 2009. "Structural characterization of human rib cage behavior under dynamic loading."  
Stapp car crash journal, 53: p. 93-125.
- [9] Poulard, D., et al., 2015. "Thoracic response targets for a computational model: A hierarchical approach to assess the biofidelity of a 50th-percentile occupant male finite element model."  
J Mech Behav Biomed Mater, 45C: p. 45-64.
- [10] Kemper, A., et al., 2005. "Biomechanical response of the human clavicle subjected to dynamic bending."  
Biomedical sciences instrumentation, 42: p. 231-236.
- [11] Duprey, S., K. Bruyere, and J.-P. Verriest, 2008. "Influence of geometrical personalization on the simulation of clavicle fractures."  
Journal of biomechanics, 41(1): p. 200-207.
- [12] Charpail, E., et al., 2005. "Characterization of PMHS Ribs: A New Test Methodology."  
Stapp car crash journal, 49: p. 183-198.
- [13] Li, Z., et al., 2010. "Rib fractures under anterior-posterior dynamic loads: experimental and finite-element study."  
Journal of biomechanics, 43(2): p. 228-234.
- [14] Li, Z., et al. 2010. "Development of finite element model of 50th percentile male using multiblock hex meshing approach."  
In Proceedings of the 6th Annual World Congress on Biomechanics, Singapore.
- [15] Guo, B.-y., et al., 2007. "Age and gender related changes in biomechanical properties of healthy human costal cartilage."  
Clinical Biomechanics, 22(3): p. 292-297.
- [16] Forman, J.L., et al. 2010. "The contribution of the perichondrium to the structural mechanical behavior of the costal-cartilage."  
Journal of biomechanical engineering, 132(9): p. 094501.
- [17] Yamada, H. and F.G. Evans, 1970. "Strength of biological materials."
- [18] Farkas, G.A., 1991. "Mechanical properties of respiratory muscles in primates."  
Respiration physiology, 86(1): p. 41-50.
- [19] Kelly, N.G., R. McCarter, and G. Barnwell, 1993. "Respiratory muscle stiffness is age- and muscle-specific."  
Aging Clinical and Experimental Research, 5(3): p. 229-238.
- [20] Kindig, M., et al., 2015. "Effect of intercostal muscle and costovertebral joint material properties on human ribcage stiffness and kinematics."  
Comput Methods Biomech Biomed Engin, 18(5): p. 556-70.
- [21] Hamzah, M., et al. 2013. "An Inverse Finite Element Approach for Estimating the Fiber Orientations in Intercostal Muscles."  
In Proceedings of the Impact Research Council on the Biomechanics of Impact (IRCOBI). Gothenburg, Sweden.
- [22] Gayzik, F.S., et al., 2009. "A multi-modality image data collection protocol for full body finite element model development."  
SAE Technical Paper.
- [23] Kindig, M.W., et al., 2010. "Structural response of cadaveric ribcages under a localized loading: stiffness and kinematic trends."  
Stapp Car Crash J, 54: p. 337-80.

- [24] Kroell, C., D. Schneider, and A. Nahum, 1971. "Impact tolerance and response of the human thorax, in biomechanics of impact injury and injury tolerances of the thorax-shoulder complex." SAE paper 710851.
- [25] Lebarbé, M. and Petit, P. 2012. "New biofidelity targets for the thorax of a 50th percentile adult male in frontal impact."  
In Proceedings of the Impact Research Council on the Biomechanics of Impact (IRCOBI).
- [26] Shaw, J.M., et al., 2006. "Oblique and lateral impact response of the PMHS thorax. " Stapp Car Crash J, 50: p. 147-167.
- [27] Kent, R., Lessley, D. and Sherwood, C. 2004. "Thoracic response to dynamic, non-impact loading from a hub, distributed belt, diagonal belt, and double diagonal belts. " Stapp Car Crash J, 48: p. 495-519.
- [28] Gehre, C., Gades, H. and Wernicke, P. 2009. "Objective rating of signals using test and simulation responses."  
In Proceeding of the 21st International Technical Conference on the Enhanced Safety of Vehicles, Stuttgart, Germany.